



Microscale phase separator for selective extraction of CO₂ from methanol solution flow



Abdolreza Fazeli, Saeed Moghaddam*

Department of Mechanical and Aerospace Engineering, University of Florida, Gainesville, FL 32611, United States

HIGHLIGHTS

- Extensive study of CO₂ separation from methanol solution using nanoporous membranes.
- Achieved a CO₂ to methanol selectivity of close to 200.
- Developed a CO₂ separator with 10 × 1 mm² membrane area for a 20 W DMFC.

ARTICLE INFO

Article history:

Received 22 May 2014

Received in revised form

17 July 2014

Accepted 22 July 2014

Available online 30 July 2014

Keywords:

Direct methanol fuel cell

Phase separation

CO₂ separation

Hydrophobic nanofibrous membrane

Portable power

ABSTRACT

This study is aimed at understanding the limits in reducing the size of a membrane-based CO₂ separator and its pressure head needs and energy consumption, while maximizing its selectivity. The separator consists of a flow channel capped by a hydrophobic nanoporous membrane through which CO₂ exits the anode flow stream of a direct methanol fuel cell (DMFC). A systematic study is conducted to determine the effect of differential pressure across the membrane, flow velocity, and flow channel dimensions on the separation process. The extraction flux was found to change linearly with pressure difference across the membrane. The effect of flow velocity on the extraction flux was negligible up to a critical velocity beyond which the separation process ceased. The separation selectivity enhanced by increasing the differential pressure across the membrane but did not change with varying the flow velocity and channel depth. Using the findings of the first part of the study, an optimal micro-separator (with a footprint of approximately 10 × 1 mm²) was designed/fabricated for a 20 W DMFC and its performance was experimentally analyzed. An unprecedented separation selectivity of close to 200 was achieved at a differential pressure of about 10 kPa and negligible energy consumption.

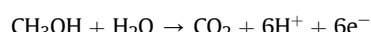
Published by Elsevier B.V.

1. Introduction

Direct methanol fuel cells (DMFCs) have been the subject of many research and development efforts over the past decade [1–4]. Although significant progress has been made, further advancements on both component and system levels are needed before small DMFCs with a higher energy density than that of small batteries can be realized. While fabrication of small-scale membrane electrode assemblies (MEAs) is widely reported in the fuel cell literature [5–9], shrinking the size of auxiliary components (i.e. pumps, valves, sensors, and flow systems) has remained a challenge [10–12]. The existing systems are bulky and expensive, primarily due to the auxiliaries designed for fuel and reactions products flow

management and dealing with deficiencies of the existing MEAs. To expand the use of DMFCs beyond the current limited military and leisure applications [13,14], compact and low-cost auxiliaries with minimal operating energy needs must be developed.

Miniaturization and performance enhancement of the anode flow system can greatly contribute toward this goal. A source of complexity in the anode flow system is production of carbon dioxide (CO₂) as a result of the following net reaction on the anode.



The generated CO₂ forms bubbles that are deleterious to the performance of DMFCs, if not properly removed from the anode electrode and discharged from the system. These bubbles can clog the anode flow channels and increase the anode pressure [15]. Increased pressure can lead to unfavorable methanol crossover [16] and increase in the pumping power required to circulate the anode

* Corresponding author.

E-mail address: saeedmog@ufl.edu (S. Moghaddam).

stream [17]. It has also been shown that the formation of large CO_2 gas bubbles at the anode reduces the effective reaction area and consequently the cell performance [18].

Numerous studies have been conducted on removal of the CO_2 bubbles from the anode flow stream. The common approach involves pumping the gas bubbles along with the fuel out of the anode electrode into a reservoir in which the bubbles are separated out from the liquid stream by the buoyancy forces [19]. Successful removal of bubbles hinges on geometrical [20–22] and surface properties [23] of the flow channel and is contingent upon the cell orientation [18,24]. Fei & Hong [24] demonstrated that buoyancy forces can outweigh the dynamic forces applied on the bubbles when the fuel cell is not vertically oriented thus leading to bubbles residing within the channels.

Citing the challenges of implementing a reservoir, Meng et al. [25] proposed a separation scheme that involved trapping bubbles within compartments formed in a microfluidic device. The bubbles were subsequently extracted from the device using porous membranes. Zhu [26] showed that hydrophobic membranes significantly outperform the hydrophilic ones in terms of separation rate (i.e. the gas exit flux). Meng et al. [27] and Meng & Kim [28] also demonstrated that hydrophobic membranes can be subjected to high differential pressures without any sign of liquid leakage. A similar approach has been reported in other studies [26,29] and different results have been reported. Notably, Zhu [26] reported that the separation rate is directly proportional to the differential pressure across the membrane.

Alternatively, non-porous membranes were used to separate CO_2 from a fuel cell system. In this approach, CO_2 must diffuse through a solid membrane instead of flowing through a porous membrane. Prakash et al. [30] studied poly(trimethylsilyl)propane (PTMSP) and polydimethylsiloxane (PDMS) membranes and determined that a PTMSP membrane exhibits a higher selectivity (defined as the ratio of CO_2 versus methanol mass transfer rate through the membrane) than a PDMS membrane. A 120- μm -thick PTMSP membrane integrated with their fuel cell system released CO_2 at a rate of $2.5 \text{ mg m}^{-2} \text{ s}^{-1}$ at a pressure difference across the membrane of 28–32 kPa, and achieved a selectivity of about 6. Further studies by Prakash & Kohl [31] showed an improvement in permeability with increase in temperature (i.e. 12.5% increase in CO_2 permeability when temperature was increased by 25 °C).

Motivated by a need to reduce the DMFCs' balance of plant (BOP), we aimed at understanding the limits in reducing the size of a membrane-based CO_2 separator and its pressure head needs and energy consumption, while maximizing its selectivity. A nano-fibrous membrane platform is used for the separation process. In the following sections, first, a systematic study on the effect of differential pressure across the membrane, flow velocity, and flow channel dimensions on the separation process are discussed. Then, using the findings of the study, an optimal micro-separator for a 20 W DMFC is designed/fabricated and its performance is experimentally analyzed.

2. Experiment

The anode flow stream is simulated through the injection of CO_2 bubbles into a 1 M methanol solution flow, while a porous PTFE membrane is bonded to the device to extract the generated CO_2 bubbles. To enable visualization of the flow stream, the device flow network is fabricated from an optically transparent material. The membrane that caps the flow network is not optically transparent.

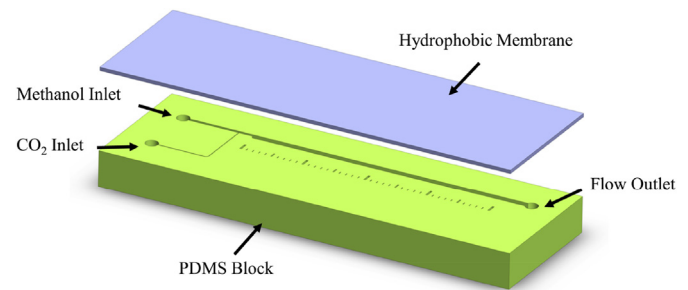


Fig. 1. A 3D schematic of the device assembly showing a PDMS block containing the flow network covered by a hydrophobic membrane.

2.1. Test device

The test device (cf. Fig. 1) is a PDMS chip bonded to a nanoporous membrane. The chip contains microchannels and connection ports for flow entry and discharge as well as pressure measurements. Methanol solution and CO_2 are injected into the device at various flow rates through a T-junction (cf. Fig. 2). The speed, size, and generation frequency of bubbles can be controlled by changing the liquid and gas flow rates [32]. Increasing the gas flow rate results in higher bubble generation frequency and a smaller bubble size (compare Fig. 2a and b). The width of the methanol and CO_2 microchannels at the T-junction is 500 and 100 μm , respectively. The main channel where the separation process takes place is 1000 μm wide and is covered by a fibrous PTFE membrane. Fig. 2c illustrates how the separation process takes place in the main channel. The studies are conducted on three devices with channel depths of 140, 300, and 500 μm . It should be noted that the height of the main and the liquid/gas channels are the same.

The PDMS chip was fabricated using a soft-lithography technique [33]. In this process, first, SU8 2050 (Microchem Co., MA) was

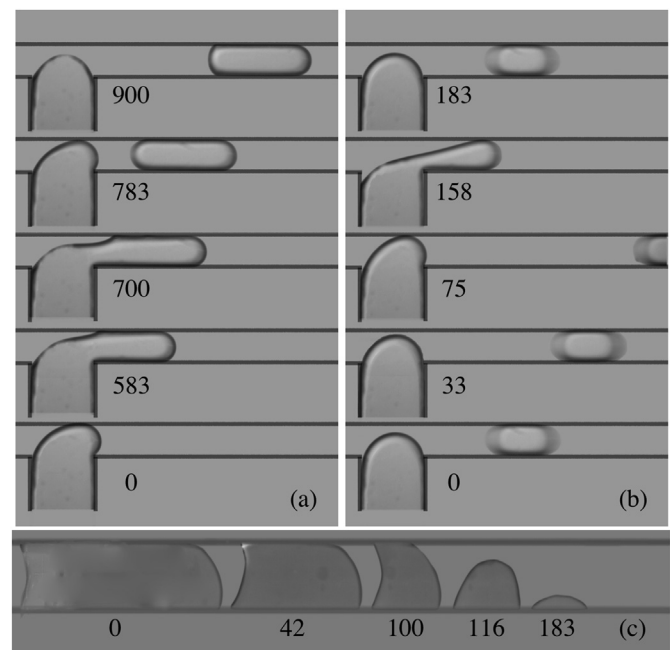


Fig. 2. (a) Slow generation of large bubbles ($Q_{\text{CO}_2} = 10 \text{ ml h}^{-1}$, $Q_{\text{methanol}} = 50 \text{ ml h}^{-1}$, $f_{\text{generation}} = 1.1 \text{ Hz}$, $V_{\text{bubble}} = 0.164 \text{ mm}^3$); (b) fast generation of small bubbles ($Q_{\text{CO}_2} = 50 \text{ ml h}^{-1}$, $Q_{\text{methanol}} = 50 \text{ ml h}^{-1}$, $f_{\text{generation}} = 5.5 \text{ Hz}$, $V_{\text{bubble}} = 0.260 \text{ mm}^3$); (c) bubble extraction process (time is in milliseconds).

spin coated on a silicon wafer and then patterned through UV light exposure and subsequent processing in SU8 developer (MicroChem Co., MA) that dissolves areas not exposed to the UV light (i.e. covered by a mask). The resulting SU8 structure served as a master mold for fabrication of the PDMS chip. PDMS pre-polymer and curing agent (SYLGARD 184 Silicone Elastomer Kit, Dow Corning, MI) were thoroughly mixed (at a ratio of 10:1) and then degassed for 30 min. The resulting liquid was poured on the silicon/SU8 mold in a glass petri dish and cured at 80 °C for 2 h on a hot plate. The cured PDMS was then cut from the mold and small holes were punched into it to provide access/connection to the microchannels. Finally, the PDMS chip was bonded to a 50-μm-thick hydrophobic nanofibrous (cf. Fig. 3) PTFE membrane (Pall Corporation, NY) with a nominal pore size of 1 μm and a porosity of 80%.

Tests are conducted at two conditions consisting of membrane facing down and up. Tests at the former configuration represents the worst case operating condition for a separator in an actual DMFC system, since the buoyancy forces do not assist with pushing the bubbles toward the membrane.

2.2. Experimental setup

The experimental setup designed to visualize the bubbles extraction process is depicted in Fig. 4. Two syringe pumps (Fisher Scientific Inc., PA) were used to deliver methanol and CO₂ to the PDMS chip. A gastight syringe (Hamilton Co., NV) was used for the gas line to ensure no leakage occurred during the experiments. A CO₂ tank was used to fill the gas syringe. The gas line was purged prior to data collection.

The pressure difference across the membrane was changed by varying the elevation of the reservoir connected to the device flow channel exit (see Fig. 4). Two PX-26 pressure transducers with $\pm 1\%$ reading error were used to measure the methanol solution and CO₂ pressures. The pressure transducers readings were recorded by an Agilent U2356A data acquisition system (Agilent Technologies Inc., CA). All experiments were conducted at room temperature ($T = 20\text{--}25\text{ }^{\circ}\text{C}$) and pressure ($P_{\text{ambient}} \approx 100\text{ kPa}$).

The flow field was imaged using a high speed Gazelle camera (Point Grey Research Inc., BC, Canada). The camera's field of view was adjusted to cover bubble-extraction area, while maintaining a sufficiently high resolution for accurate measurement of the size of bubbles. Streampix5 software (Norpix Inc., Quebec) was used to record images captured by the camera. An MI150 high intensity light source (Dolan-Jenner Ind., MA) was used to illuminate the flow field.

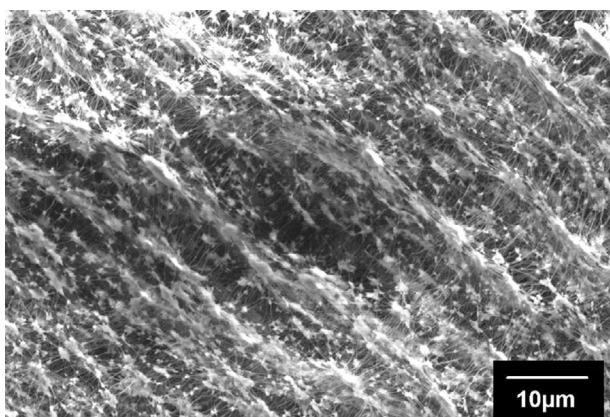


Fig. 3. SEM micrograph of nano-fibrous PTFE membrane.

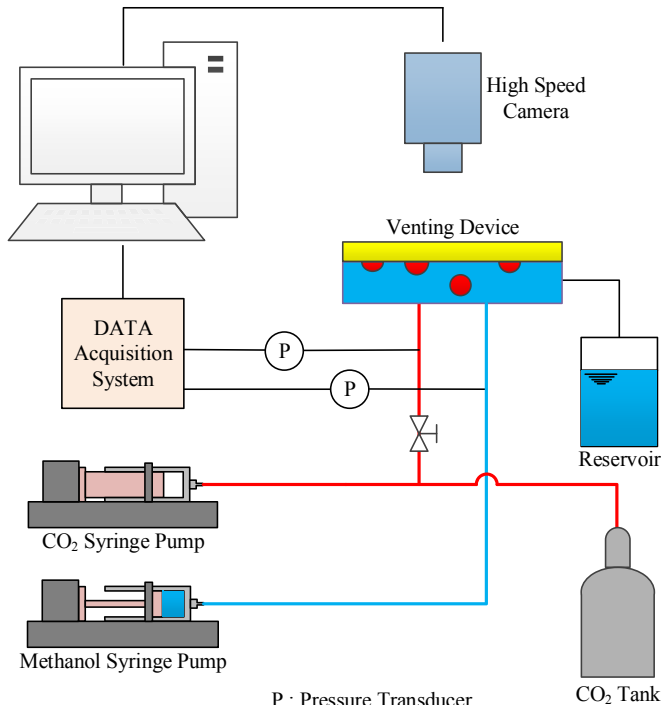


Fig. 4. A schematic of the experimental setup depicting the test device and flow injection system as well as the imaging and data recording system.

The bubble images were captured at three different cross sections (cf. Fig. 5a). The obtained images were processed in a multi-step procedure. First, the bubble boundaries were identified by the MATLAB® software (Mathworks Inc., MA), using an intensity-based edge detection scheme, and the background was removed (cf. Fig. 5b). Finally, using the images, the bubble was reconstructed and the change in its volume (i.e. the extraction rate) was calculated (cf. Fig. 5c).

3. Results and discussion

Several experiments were conducted in order to understand the effect of important parameters on the extraction rate of bubbles through the membrane. A parametric study was performed to determine the effect of pressure difference across the membrane, methanol solution and gas flow rates, and the channel depth on extraction flux of CO₂ through the membrane. At each test condition, to ensure that the flow has reached a steady state (when the bubbles size did not change after the T-junction), videos were recorded until at least 500 s.

3.1. Effect of differential pressure

The methanol solution and CO₂ flow rates were kept constant at 10 ml h⁻¹ and 25 ml h⁻¹, respectively, to ensure a similar flow condition (i.e. bubble velocity and size) between all tests. Fig. 6 depicts the extraction process of CO₂ bubbles through the membrane at two different pressures. Each image sequence shows changes in the bubble size as it continuously vents through the membrane. Comparison of the time of extraction between the two cases (i.e. 1.7 kPa and 4.1 kPa differential pressures) clearly indicates that increasing the pressure shortens the bubble venting time (from 160 ms to less than 50 ms).

Fig. 7 provides quantitative data on the effect of differential pressure on the extraction rate. Fig. 7a shows the extraction rate as

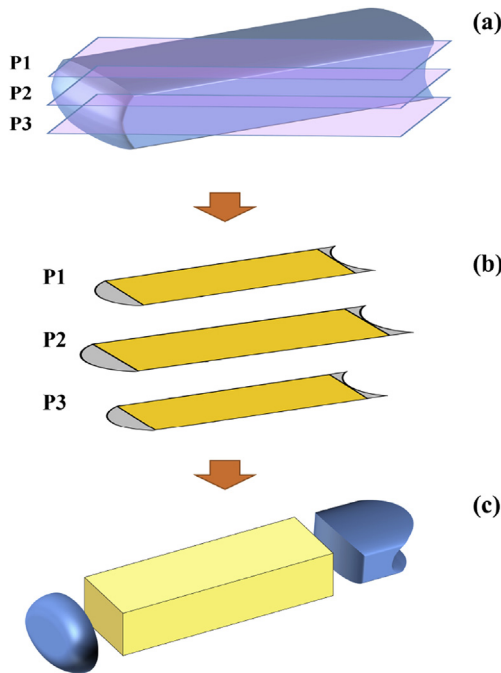


Fig. 5. (a) 3D schematic of a typical bubble, (b) bubble cross-section at three different elevations, and (c) reconstructed bubble.

a function of time at three different pressures. The results suggest that the extraction rate rapidly declines with time. A decrease in the contact area of the bubble and membrane was considered a major factor responsible for the observed behavior. To exclude the effect of this factor, the extraction flux (i.e. extraction rate divided by the area of the bubble in contact with the membrane) was calculated (cf. Fig. 7a). The results confirm that the extraction flux does not change with time and bubble-membrane contact area. Finally, the bubbles extraction flux at all tests was calculated and plotted versus the differential pressure. The results (cf. Fig. 7b) suggest that the extraction flux increases linearly when the differential pressure across the membrane is increased.

3.2. Effect of velocity

In a second set of tests, the effect of methanol solution velocity on the bubbles extraction flux was studied. The measurements were first conducted at a differential pressure of 3.0 kPa. Fig. 8 provides the results. The data suggest that increasing the velocity results in a decline in the bubbles extraction flux. Increase in the flow pressure drop was identified as a cause of the observed

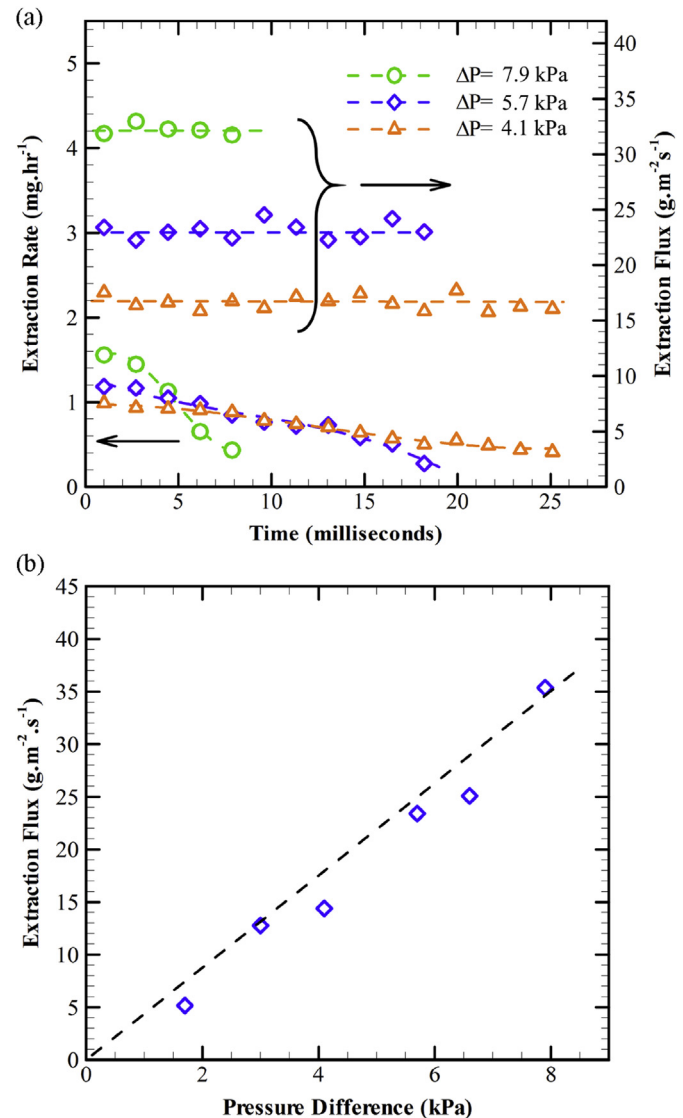


Fig. 7. (a) Extraction rate and extraction flux as a function of time at three different differential pressures and (b) effect of pressure difference across the membrane on extraction flux (microchannel depth is 300 μ m).

behavior, since it lowers the differential pressure responsible for driving the bubbles through the membrane. Results of an additional test at a higher differential pressure of 5.7 kPa demonstrate this effect (cf. Fig. 8). A lesser decline in the extraction flux compared to tests conducted at 3.0 kPa differential pressure was achieved. This is

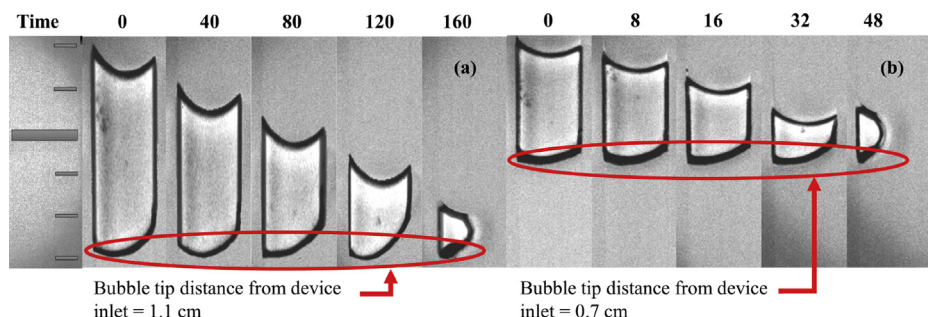


Fig. 6. Bubble images during the extraction process at different differential pressures across the membrane: (a) $\Delta P = 1.7$ kPa and (b) $\Delta P = 4.1$ kPa. Time is in milliseconds. Scale is in millimeters.

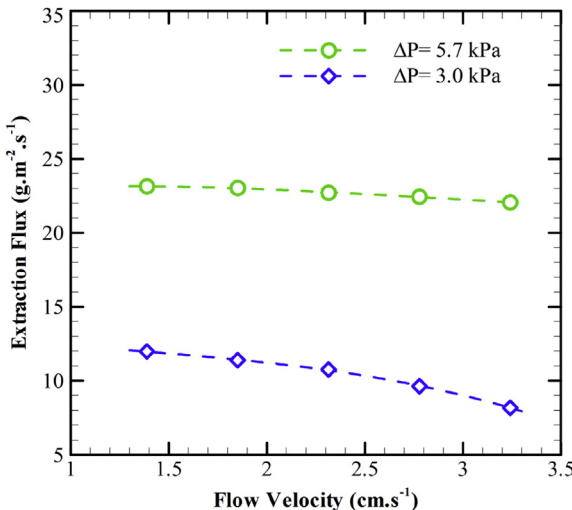


Fig. 8. Extraction flux as a function of flow velocity at two different differential pressures.

because the flow pressure drop is a smaller fraction of the 5.7 kPa differential pressure.

These measurements suggest that flow velocity does not significantly change the extraction flux as long as a sufficient pressure difference across the membrane is maintained. In a fuel cell system, this phenomenon can lead to a self-controlled process, in which an increase in system pressure, due to the accumulation of CO_2 bubbles, enhances the extraction flux.

3.3. Operational limits

When the methanol solution (i.e. fuel) supply velocity exceeded a certain limit, a fraction of bubbles ceased to exit the flow through the membrane. This phenomenon is depicted in Fig. 9 that shows a small bubble flowing along the channel without any change in its volume. This phenomena has also been observed in prior studies [34,35], and formation of a thin liquid layer between the bubbles and the membrane has been identified as its cause. To better understand the implications of this phenomenon on the design of a device, a set of tests was conducted. The initial measurements were conducted with the device oriented such that the membrane faced down. As mentioned earlier, this configuration represents the most critical operating condition of the device, since gravity does not

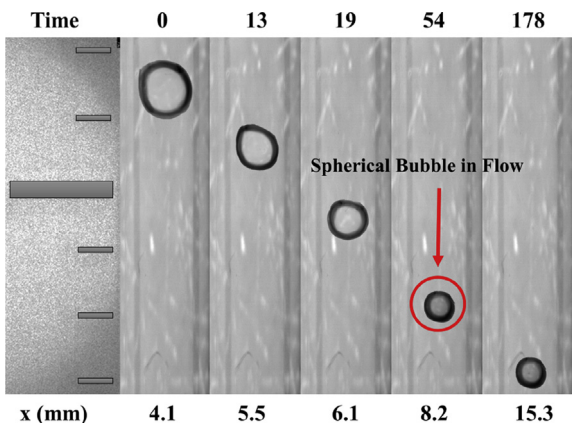


Fig. 9. Images showing extraction process of a bubble until it reached a certain size at which the extraction process ceased. "x" represents distance from the flow channel inlet. Time is in milliseconds. Scale is in millimeters.

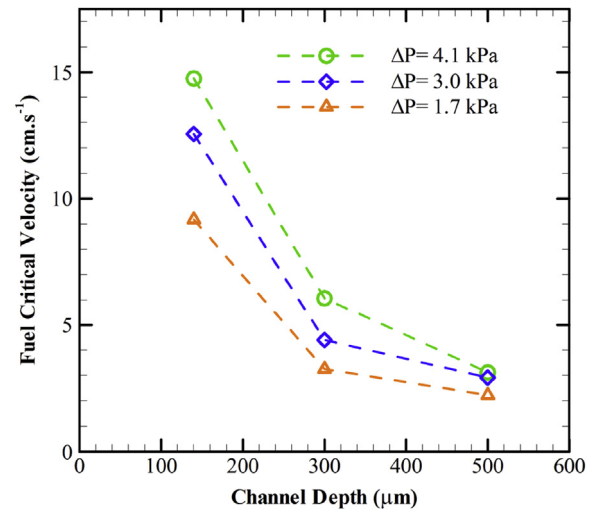


Fig. 10. Effect of channel height on critical velocity at different differential pressures, while the membrane is facing down.

assist with pushing bubbles against the membrane. At this test configuration, the critical velocity significantly declined as the channel depth was increased (cf. Fig. 10). For example, increasing the channel depth from 130 microns to 500 microns resulted in a decrease of 78% in the critical velocity. The device orientation was then changed such that the membrane faced upward, and the tests were repeated. The results (cf. Fig. 11) showed that the impact of channel depth on the critical velocity is minimal under this test condition.

Comparison of the results of the two test sets suggested that gravity greatly facilitates separation of bubbles from the membrane. Bubbles experience a buoyancy force proportional to their volume. For example, a 500 microns bubble experiences an approximately 57 times larger buoyancy force than a 130 microns bubble. In deep channels, when the bubble diameter reduces below the channel depth while the membrane is facing down, a large buoyancy force assists separation of bubbles from the membrane at low fluid velocities. In shallow channels, the buoyancy force is too small to impact the force balance on a bubble.

3.4. Selectivity and fuel efficiency

The most important factor in the design of a CO_2 venting device is its selectivity. The device should be more selective to CO_2 than the fuel to minimize the system fuel loss. The nanoporous membrane allows convective flux of the gas phase while it limits the fuel permeation to diffusive transport (cf. Fig. 12). Depending on the velocity, convective transport can be orders of magnitude faster than the diffusive transport. In a non-porous membrane, however, the transport mechanism of species is diffusive, and a high selectivity can be achieved only if the membrane material has a high CO_2 diffusion coefficient and a low methanol diffusion coefficient.

To determine the membrane selectivity, a gravimetric method is utilized to measure the fuel loss rate. In this method, the fuel pumped into the venting device is collected and its weight is measured. The weight difference between the pumped and collected fuel is considered to be the fuel loss through the membrane. The weight measurements were conducted using a precision balance (Mettler Toledo AL104, MA) with an accuracy of 0.0001 g. To evaluate the accuracy of this method, the flow channel was covered with a Kapton tape to block mass transfer. During three separate tests, 18–20 g fuel was pumped into the device and

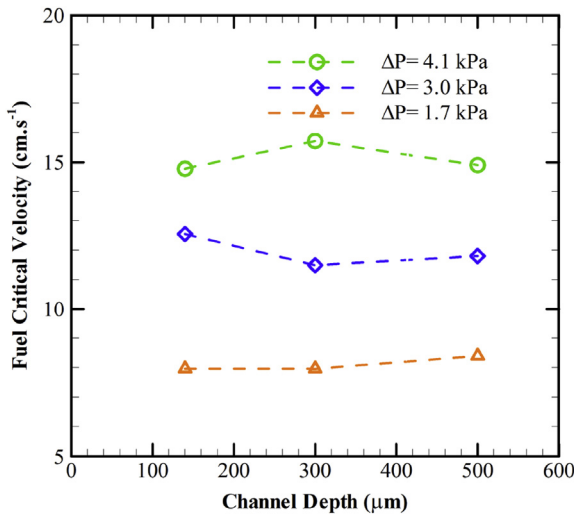


Fig. 11. Effect of channel height on critical velocity at different differential pressures, while membrane is facing up.

collected at the exit. The net change in the weight of the fluid was between 0.001 and 0.003 g.

Several tests were conducted to investigate the effect of pressure difference across the membrane, fuel velocity, and channel depth on the fuel loss rate. Fig. 13 shows the fuel loss rate as a function of flow velocity in channels with different depths. The results indicated that the fuel loss rate is nearly constant (i.e. it is independent of the flow velocity and channel depth). This suggests that fuel loss occurs via diffusion of the fuel molecule through the membrane. To put the results in perspective, we define fuel efficiency as the ratio of fuel flow rate to the fuel loss rate:

$$\text{Fuel Efficiency} = \text{Fuel Flow Rate (mg s}^{-1}\text{)}/\text{Fuel Loss Rate (mg s}^{-1}\text{)}$$

Since the fuel loss rate is independent of the flow velocity and channel depth, the fuel efficiency improves as the flow velocity and

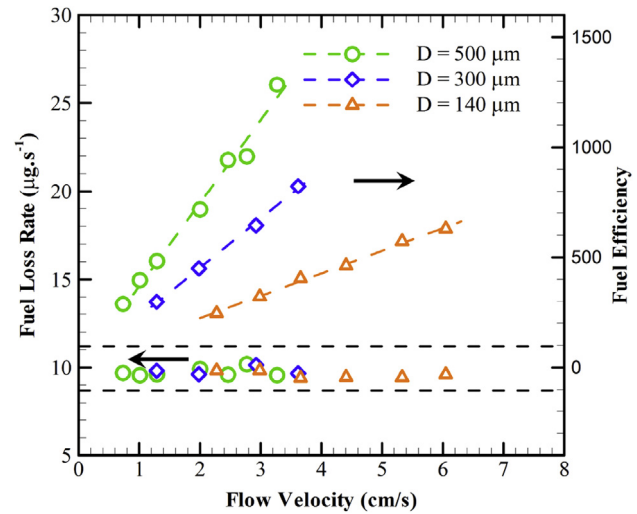


Fig. 13. Fuel loss rate and fuel efficiency as a function of flow velocity and channel depth ($\Delta P = 5.7$ kPa).

channel depth are increased (cf. Fig. 13). However, as mentioned earlier, variations of these parameters greatly impact the venting process. Thus, a more suitable parameter for evaluation of the device performance is selectivity, defined as:

$$\text{Selectivity} = \text{CO}_2 \text{ Venting Rate (g m}^{-2} \text{s}^{-1}\text{)}/\text{Fuel Loss Rate (g m}^{-2} \text{s}^{-1}\text{)}$$

Fig. 14 provides data on the membrane selectivity as a function of flow velocity and differential pressure across the membrane. The results show that selectivity is independent of the device operating velocity. However, it is a strong function of differential pressure across the membrane. The results also suggest that 1–2 orders of magnitude higher selectivity at an order of magnitude lower differential pressure across the membrane compared to prior studies [30,31] is achieved.

3.5. Venting device for a 20 W DMFC system

The results determined in the previous sections are utilized to design a CO_2 venting device for a 20 W DMFC system. Fuel flow and

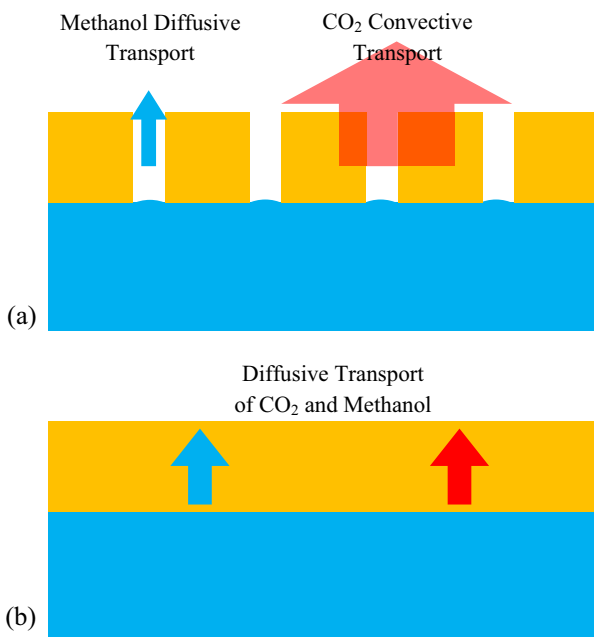


Fig. 12. Gas and liquid permeation through different membranes (a) porous (b) non-porous.

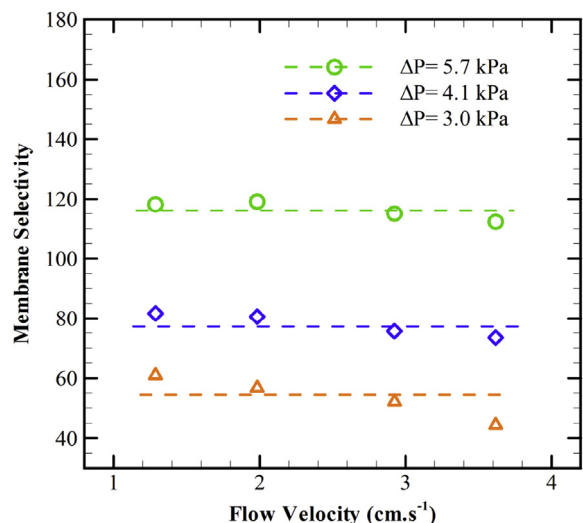


Fig. 14. Fuel efficiency as a function of flow velocity at different differential pressures (microchannel depth is 300 μm).

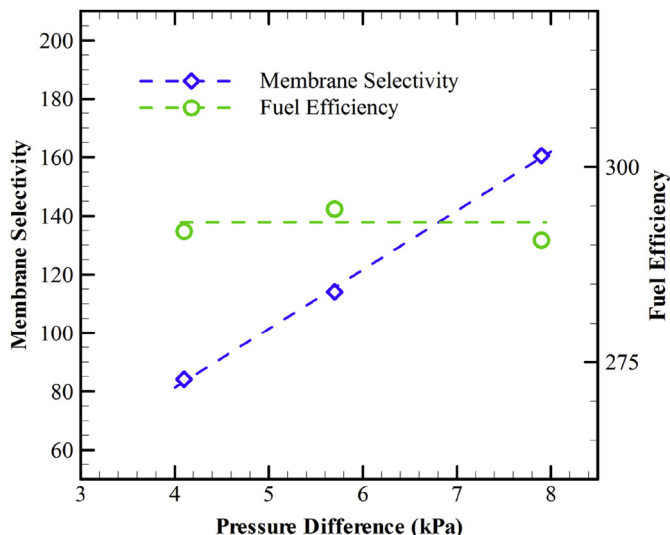


Fig. 15. Selectivity and fuel efficiency of venting device as a function of differential pressure for a 20 W DMFC.

CO_2 production rates of 11.22 ml h^{-1} and 4.5 mg s^{-1} , respectively, are used for the system [36]. A device with a venting section of $10 \times 1 \text{ mm}^2$ and a flow channel depth of 300 microns is designed and fabricated.

Fig. 15 provides test data on selectivity and fuel efficiency of the device over an operating pressure range of 4–8 kPa. The device selectivity increases with pressure and reaches to almost 160 at the optimal condition where the pressure difference across the membrane and extraction flux are 7.9 kPa and $35.4 \text{ g m}^{-2} \text{ s}^{-1}$, respectively. This selectivity level is two orders of magnitude higher than the alternative approaches [30,31]. The device operates at a fuel efficiency of about 300. The device theoretical power consumption, calculated based on the fuel flow rate and pressure drop along the microchannel, is only 5 μWh .

4. Conclusion

The separation process of gas bubbles from the methanol–water solution through a hydrophobic nanoporous membrane was studied. The differential pressure across the membrane was found to be the most important factor in the separation process, and its increase linearly enhanced the separation rate. When the membrane faced down, at a critical velocity, a fraction of bubbles ceased to exit the flow through the membrane. Increasing the channel depth from 130 microns to 500 microns resulted in a major decrease of 78% in the critical velocity. The results suggested that in deep channels, when the bubble diameter reduces below the channel depth, a large buoyancy force assists separation of bubbles from the membrane at low fluid velocities. In shallow channels, the buoyancy force is too small to impact the force balance on a bubble.

Measurements of the fuel loss rate suggested that the primary loss mechanism is diffusion through the membrane. Because the fuel diffusion rate is independent of the flow velocity and channel depth, their enhancement increases the fuel efficiency. However,

the upper limits of these parameters are dictated by the physics of the separation process (i.e. a significant drop in critical velocity as a result of an increase in channel depth). Since increasing the differential pressure across the membrane linearly enhanced the bubbles extraction flux without impacting the fuel loss rate, the device selectivity improved when the differential pressure was increased.

These parametric studies provided in depth understanding of the parameters affecting the separation process as well as the operational limits and enables development of highly selective compact micro-separators.

References

- [1] S.-H. Liu, W.-Y. Yu, C.-H. Chen, A.-Y. Lo, B.-J. Hwang, S.-H. Chien, S.-B. Liu, *Chem. Mater.* 20 (2008) 1622–1628.
- [2] S.K. Kamarudin, F. Achmad, W.R.W. Daud, *Int. J. Hydrogen Energy* 34 (2009) 6902–6916.
- [3] A. Schröder, K. Wippermann, W. Lehnert, D. Stolten, T. Sanders, T. Baumhöfer, N. Kardjilov, A. Hilger, J. Banhart, I. Manke, *J. Power Sources* 195 (2010) 4765–4771.
- [4] L. Feng, J. Zhang, W. Cai, W. Xing, C. Liu, *J. Power Sources* 196 (2011) 2750–2753.
- [5] K. Shah, W.C. Shin, R.S. Besser, *Sens. Actuators B Chem.* 97 (2004) 157–167.
- [6] G.Q. Lu, C.Y. Wang, T.J. Yen, X. Zhang, *Electrochim. Acta* 49 (2004) 821–828.
- [7] J. Yeom, G.Z. Mozsgai, B.R. Flachsbart, E.R. Choban, A. Asthana, M.A. Shannon, P.J.A. Kenis, *Sens. Actuators B Chem.* 107 (2005) 882–891.
- [8] S.-C. Yao, X. Tang, C.-C. Hsieh, Y. Alyousef, M. Vladimer, G.K. Fedder, C.H. Amon, *Energy* 31 (2006) 636–649.
- [9] S. Moghaddam, E. Pengwang, Y.-B. Jiang, A.R. Garcia, D.J. Burnett, C.J. Brinker, R.I. Masel, M.A. Shannon, *Nat. Nanotechnol.* 5 (2010) 230–236.
- [10] S.K. Kamarudin, W.R.W. Daud, S.L. Ho, U.A. Hasran, *J. Power Sources* 163 (2007) 743–754.
- [11] S. Moghaddam, E. Pengwang, R.I. Masel, M.A. Shannon, *J. Power Sources* 185 (2008) 445–450.
- [12] S. Moghaddam, E. Pengwang, R.I. Masel, M. Shannon, *J. Power Sources* 195 (2010) 1866–1871.
- [13] P. Podesser, in: *Small Fuel Cells 2009 11TH Annu. Int. Conf. Portable Micro Fuel Cells Commer. Mil. Appl.*, Orlando, 2009.
- [14] H. Merhoff, P. Helbig, in: *Small Fuel Cells 2009 11TH Annu. Int. Conf. Portable Micro Fuel Cells Commer. Mil. Appl.*, Orlando, 2009.
- [15] X. Li, *Principles of Fuel Cells*, Taylor & Francis Group, 2005.
- [16] M. Hogarth, in: G. Hoogers (Ed.), *Fuel Cell Technol. Handb.*, CRC Press LLC, Boca Raton, 2003.
- [17] S. Sundarraj, S.I. Allakhverdiev, S. Ramakrishna, *Int. J. Hydrogen Energy* 37 (2012) 8765–8786.
- [18] H. Yang, T.S. Zhao, Q. Ye, *J. Power Sources* 139 (2005) 79–90.
- [19] G. Hoogers, *Fuel Cell Technology Handbook*, CRC, Boca Raton, Florida, 2002.
- [20] K. Fei, W.H. Chen, C.W. Hong, *Microfluid. Nanofluidics* 5 (2007) 119–129.
- [21] P. Argyropoulos, K. Scott, W.M. Taama, *Electrochim. Acta* 44 (1999) 3575–3584.
- [22] T. Bewer, T. Beckmann, H. Dohle, J. Mergel, D. Stolten, *J. Power Sources* 125 (2004) 1–9.
- [23] K. Fei, C.H. Cheng, C.W. Hong, *J. Fuel Cell Sci. Technol.* 3 (2006) 180–187.
- [24] K. Fei, C.W. Hong, *Microfluid. Nanofluidics* 3 (2007) 77–88.
- [25] D.D. Meng, J. Kim, C.-J. Kim, *J. Micromech. Microeng.* 16 (2006) 419–424.
- [26] X. Zhu, *Microsyst. Technol.* 15 (2009) 1459–1465.
- [27] D.D. Meng, T. Cubaud, C.-M. Ho, C.-J. Kim, *Microelectromech. Syst. J.* 16 (2007) 1403–1410.
- [28] D.D. Meng, C.J. Kim, *J. Power Sources* 194 (2009) 445–450.
- [29] M. Kraus, U. Krewer, *Sep. Purif. Technol.* 81 (2011) 347–356.
- [30] S. Prakash, W. Mustain, P.A. Kohl, *J. Power Sources* 185 (2008) 392–400.
- [31] S. Prakash, P.A. Kohl, *J. Power Sources* 192 (2009) 429–434.
- [32] P. Garstecki, M.J. Fuerstman, H.A. Stone, G.M. Whitesides, *Lab Chip* 6 (2006) 437–446.
- [33] D. Qin, Y. Xia, G.M. Whitesides, *Nat. Protoc.* 5 (2010) 491–502.
- [34] P.G. De Gennes, F. Brochard-Wyart, D. Quéré, *Capillarity and Wetting Phenomena: Drops, Bubbles, Pearls, Waves*, Springer, 2003.
- [35] J. Xu, R. Vaillant, D. Attinger, *Microfluid. Nanofluidics* 9 (2010) 765–772.
- [36] R. Rashidi, I. Dincer, G.F. Naterer, P. Berg, *J. Power Sources* 187 (2009) 509–516.